

# CONTINUOUS DYNAMIC RECRYSTALLIZATION OF EXTRUDED NiAl POLYCRYSTALS DURING SUPERPLASTIC DEFORMATION PROCESS

Guo JianTing \*, Du Xing Hao \*, Li Gusong\*

\* Superalloy Department of Institute of Metal Research, The Chinese Academy of Sciences

**Keywords:** NiAl, Superplasticity, continuous dynamic recrystallization

## Abstract

The tensile deformation behavior and the associated deformation microstructures of extruded NiAl polycrystals with stoichiometric composition were systemically investigated under various conditions of temperature and strain rate by means of optical microscopy (OM), electron backscattered diffraction (EBSD) and transmission electron microscopy (TEM). Consequently, the superplastic deformation behavior with elongations over 200% and strain rate sensitivity indexes near to 0.30 was observed at high temperatures, i.e. at 1273–1373 K and a wide strain rate range from  $10^{-4} s^{-1}$  to  $10^{-1} s^{-1}$ . The deformation microstructures responsible for the large tensile elongation consisted of subgrains, low angle grains as well as high angle grains, and indicated that a continuous dynamic recrystallization (CDRX) process was operating. It is suggested that comparable work hardening (by the glide motion of  $\langle 001 \rangle$  type dislocations) with the dynamic accommodation mechanism (CDRX) took place, and led to a steadily increased flow stress and a favorable value of strain rate sensitivity, resulting in superplastic elongation and high fracture resistance.

## 1 Introduction

Intermetallic compound of NiAl with B2 crystal structure is regarded as a potential candidate of high temperature structural materials because it offers a wide range of attractive mechanical, chemical and physical properties, such as high

melting point, low density, good thermal conductivity and high stiffness [1,2]. However, it exhibits inherently brittle fracture and zero ductility at ambient temperatures, and its use as engineering materials is restricted in many cases by its poor fracture resistance and limited fabricability. In an attempt to improve the ductility of single phase NiAl, the tensile behavior of NiAl has been investigated at wide ranges of temperatures and strain rates using polycrystals [3,4] and single crystals [5-7]. In addition, the deformation of NiAl by compression has been studied [8-10]. Some interesting results were disclosed by these studies. For NiAl single crystals with various kinds of orientation, the anomalously large tensile elongation like almost the superplastic deformation has been observed to take place at a very limited temperature regime of  $0.35 \sim 0.40 T_m$ . For NiAl polycrystals, extruded NiAl underwent obvious a brittle to ductile transition at about 400 °C and exhibited superplasticity at temperatures ranging from 1000 °C to 1100 °C under initial strain rates of  $1.67 \times 10^{-4} \sim 1.67 \times 10^{-2} s^{-1}$  [4,11]. There were substantial evidences indicating that details of the dislocation structure play a central role in determining the deformation behavior of NiAl [1,2,12,13]. At room temperature and below NiAl deformed almost exclusively by the motion of  $\langle 100 \rangle$  dislocations whose Burgers vector gives only three independent slip systems. At intermediate temperatures, where a brittle to ductile transition occurred,  $\langle 110 \rangle$  dislocations began to contribute to the plastic deformation [13]. The superplasticity observed at high temperatures

was ascribed to the process of dynamic recovery and recrystallization, but the authors did not definitely elucidate the role of dislocations during superplastic deformation [11].

Most recently, the authors discovered that extruded NiAl exhibited superplastic deformation even at high strain rate ( $10^{-1} \text{ s}^{-1}$ ) at high temperatures, which could be used directly by conventional industry, such as forging. The discovery makes it possible for the components of brittle NiAl materials to be synthesized by superplastic forming methods in one step. So it is important to understand furthermore the mechanism of superplastic deformation at high temperatures. In this paper, the superplastic deformation behavior is systemically characterized and the deformation mechanism is clarified by means of optical microscopy (OM), electron backscattered diffraction (EBSD) and transmission electron microscopy (TEM). It appeared that grain boundary formation was accomplished by gradual conversion of subgrain boundaries into high angle grain boundaries through continuous dynamic recrystallization (CDRX). CDRX in B2-type ordered NiAl during superplasticity deformation is determined by its unique physical properties, i.e. very high stacking-fault energy (SFE). The relationship between superplastic deformation and CDRX is also discussed in the present paper.

## 2 Experimental Procedure

Ingots of stoichiometric NiAl with 100 mm in diameter and height of 120mm were induction melted under vacuum conditions. These cast ingots were canned with mild steel and extruded at about 1000 using 16:1 reduction in area followed by cooling in air. The steel can was removed by pickling the extruded bars in a solution of 30% $\text{HNO}_3$ +30%HCL+40% $\text{H}_2\text{O}$  (volume fraction). After pickling was completed, the rods were stress-relieved by annealing for 1 hour at 1173 K. The flat tensile specimens, having a gauge section of 2.5 mm  $\times$  2 mm  $\times$  10 mm, were electro-discharge machined from the rods with the gauge length parallel to the extrusion direction. Tensile tests were

performed on a SHIMADZU AG-250 KNE testing machine at 800~1373 K under initial strain rates ranging  $1.67 \times 10^{-4}$ ~ $1.67 \times 10^{-1} \text{ s}^{-1}$ . Tensile loads were automatically recorded through a supplementary computer, true stress-true strain curves were drawn from data recorded by the computer under the assumption of volume constancy. To investigate the microstructural change, some specimens having a gauge section of 5mm  $\times$  2mm  $\times$  10mm were deformed to a prescribed strain, then unloaded and water quenched as quickly as possible. The foils for TEM observation were produced by the conventional twin jet polishing technique using an electrolyte of 10% perchloric acid in methanol at 253 K after mechanical polishing to 100 $\mu\text{m}$ . The samples were examined in a Philips TEM 420 analytical electron microscope operated at 150kv. EBSD was carried out in a Cambridge 360 scanning electron microscope with a TSL automated orientation imaging microscopy (OIM) attachment. OIM scans were carried out by beam scanning method using 1  $\mu\text{m}$  step size over areas from 150  $\times$  200  $\mu\text{m}^2$ . OIM data were analyzed using Channel 4 software of HKL Technology Company.

## 3 Results

### 3.1 Mechanical properties

#### 3.1.1 The elongation behavior

The elongations of the extruded NiAl polycrystals were investigated as a function of temperature and strain rate and the results were shown in Fig.1. At low temperature till to near 400 K the elongations were almost zero under the testing strain rates. However, it is evident that elongation value increased dramatically when the testing temperatures were fallen into the ranges of 500~800 K and 1273~1373 K. It has well established that the rapid increase of elongation value at intermediate temperatures can be ascribed to the brittle-to-ductile transition for NiAl and many mechanisms responsible to the change have been suggested, such as the advent of <110> dislocations [13] or

the operation of a short-circuit diffusion process [4]. It is interesting that the superplastic elongation values ( $\delta > 200\%$ ) were obtained in the second temperature ranges even under the high strain rate ( $10^{-1} s^{-1}$ ). The discovery is of significance since the elongation beyond 200% is sufficient to make, using superplastic forming technology, extremely complex shapes for NiAl material [14]. Figure 2 showed the macrograph of specimens tested at 1323 K and 1373 K under the strain rate of  $1.67 \times 10^{-1} s^{-1}$ . The result revealed that these specimens deformed even to fracture without obvious necking, which is similar to the character of superplastic deformation of many metal based alloys [14].

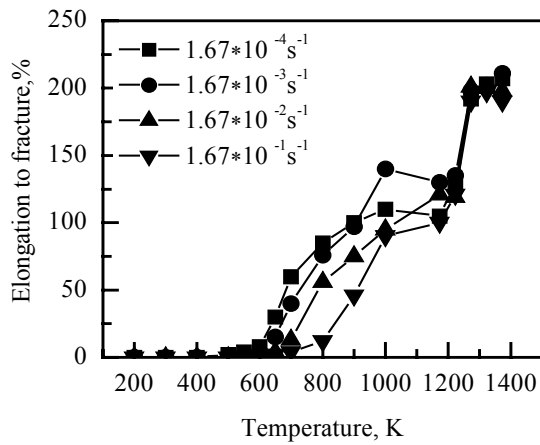


Fig.1. The elongation value of extruded NiAl as a function of strain rate at different temperatures

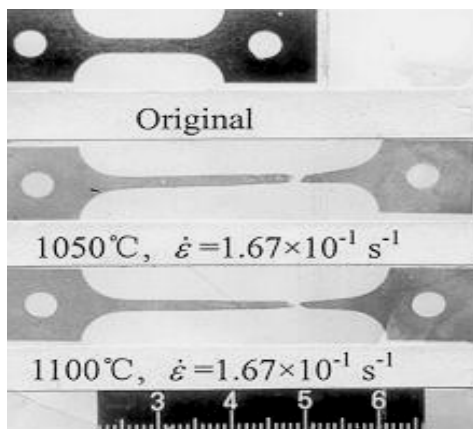


Fig.2. A direct comparison of superplastically deformed NiAl samples with original sample

### 3.1.2 Stress-strain behavior

To characterize the deformation behavior of the alloy true stress versus true strain curves were plotted, which were based on the assumption of uniform deformation. Fig.3 (a) illustrates the true stress versus true strain curves of NiAl deformed at different strain rates at 1373 K. It clearly shows that at high strain rates, the true stress–true strain curves exhibit a continuous increase of stress up to high strain (0.60), followed by a relatively rapid decrease of stress. At the lower strain rates, the flow stress decreases and the strain of steady flow increases. The extended steady flow behavior indicated uniform plastic deformation up to large strains without fracturing and therefore good necking resistance of the tested specimens. The influence of temperature was similar to that of the influence of strain rate; an increase in temperature led to the same pattern in the true stress–true strain curves as that observed by a decrease of strain rate (Fig.3(b)).

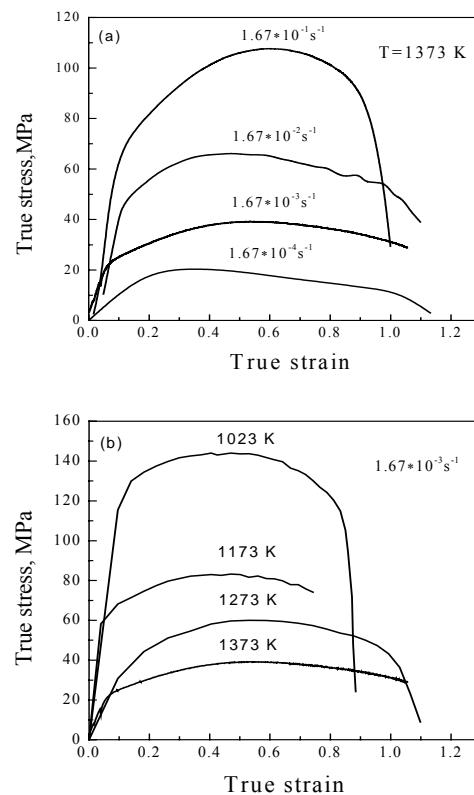


Fig.3. True stress versus true strain over a range of strain rates at 1373 K (a) and over a range of temperatures at  $1.67 \times 10^{-3} s^{-1}$  for samples processed by cast and extrusion

### 3.1.3 Constitutive equation

High temperature deformation of materials under steady-state conditions can generally be expressed by the relation between flow stress ( $\sigma$ ) and strain rate ( $\dot{\epsilon}$ ):

$$\dot{\epsilon} = A\sigma^n \exp(-Q/RT) \quad (1)$$

where  $A$  is a constant,  $n$  is the stress exponent being identical to  $1/m$  ( $m$  is the strain rate sensitivity index),  $Q$  is the apparent activation energy,  $R$  is a gas constant and  $T$  is the thermodynamic temperature. Fig.4 shows the relationship between the flow stress (the peak stress) and the strain rate for NiAl at various temperatures. Linear relationships are found for NiAl at each temperature. Generally, the strain rate sensitivity index increased with increasing temperature and attained 0.30 above 1273 K. It is interesting that the strain rate sensitivity indexes were kept at approximately 0.30 for the strain rate range measured even at very high strain rate ( $10^{-1} \text{ s}^{-1}$ ). According to Nieh et al [15], a value of  $m=0.30$  was common to some superplastic intermetallics, such as FeAl, Fe<sub>3</sub>Al and Ti<sub>3</sub>Al.

From equation (1) it can be shown that:

$$Q = n \cdot R \cdot \frac{\partial \ln \sigma}{\partial (1/T)} \quad (2)$$

where  $n=1/m$ . Fig.5 shows an Arrhenius plot for the flow stress of the tested NiAl where the peak stresses in the true stress-true strain curves were used as the flow stress. The plot was performed for the high strain rate of  $1.67 \times 10^{-1} \text{ s}^{-1}$ . Strictly speaking, linear relationship was not defined for NiAl at the tested strain rate. The estimated apparent activation energy was calculated to be about 260 kJ/mol at high temperature (i.e. 1273~1373 k) and 225 kJ/mol at low temperature (i.e. 1173~1273K) based on the equation (2). These values of activation energy are all fallen into the range of value (220~300 kJ/mol) measured in creep deformation of NiAl and also are corresponding to the diffusion energy of vacancies in NiAl [2].

## 3.2 Microstructural evolution

### 3.2.1 OM observations

Metallographic examination shows that the mean grain size in the gauge section of the tensile specimens fluctuated dramatically with the increase of strain. Fig.6 provides an example, in which the mean grain size of NiAl decreased from about 150  $\mu\text{m}$  at elongations of 40% to 40

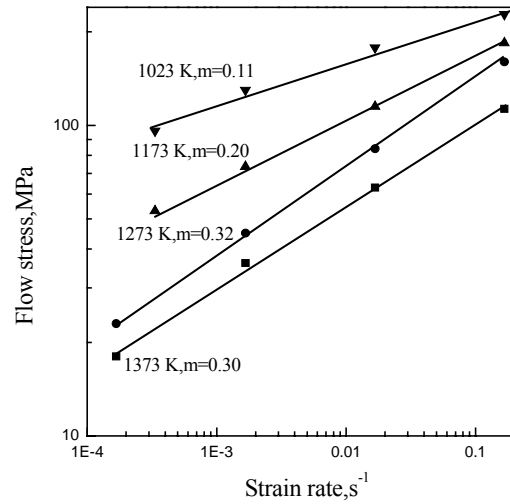


Fig.4. Relations between the flow stress and the strain rate for NiAl. Note that the peak stresses in the stress-strain curves were used as the flow stress.

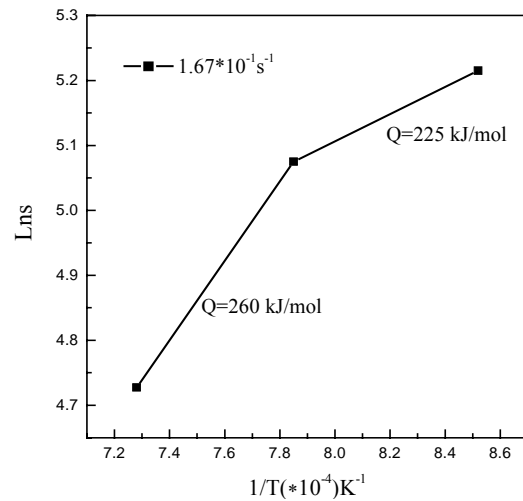


Fig.5. Arrhenius plots for the flow stress of NiAl at a strain rate of  $1.67 \times 10^{-1} \text{ s}^{-1}$ . Note that the peak stress in the true strain-true stress curves were used as the flow stress.

$\mu\text{m}$  at elongation of 100% but increased to about 100 $\mu\text{m}$  at 210%. Fig.6 (a) shows that the grain boundaries appeared slightly splintery and a few recrystallized grains emerged near the original boundaries. With the deformation all grain boundaries became more flexuous and more convex parts of the grain boundaries separated from the original grains and then became new small equiaxial grains. On the other hand, new small equiaxial grains also formed inside the original grains. Fig. 6 (b) shows that most of grains of NiAl were fine and equiaxial during the deformation process.

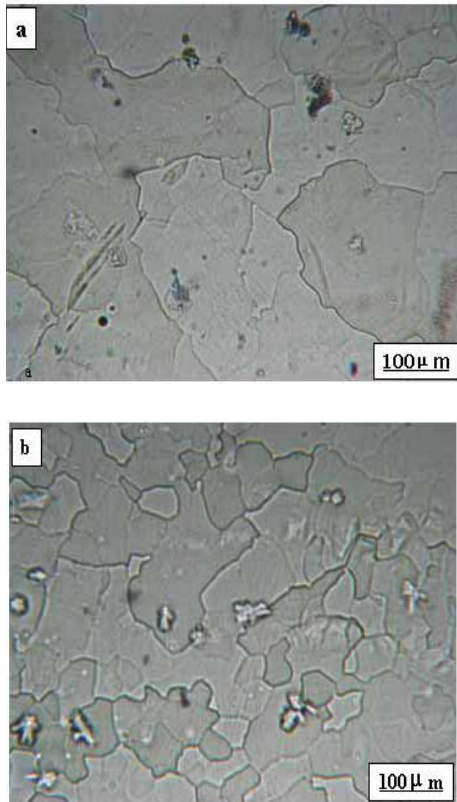


Fig.6. Microstructure evolution of NiAl during superplastic deformation ( $\dot{\epsilon}=1.67 \times 10^{-3} \text{ s}^{-1}$ ,  $T=1373 \text{ K}$ ): (a)  $\delta=40\%$ ; (b)  $\delta=210\%$  ( $\delta$ : Elongation, %)

### 3.2.2 TEM observations

Fig. 7 shows the dislocation structure and subgrains configuration in the sample deformed at 1373 K with the tensile elongation of 40%. Fig.7 (a) showed that the configuration of randomly distributed dislocations and dislocation array in the deformed sample. The density of dislocations in the grains was high, demonstrating that dislocation glide behavior dominated the whole deformation process. The “A” site shows the arched dislocation shape, indicating that dislocation climb behavior has occurred. Fig.7 (b) shows that the recrystallized grain boundaries were composed of edge dislocations, i.e. a dislocations wall or a dislocation network. Fig. 8 shows a high angle boundary (a) and a convex subboundary (b) in the sample deformed at 1373 K with the tensile elongation of 210%, which showed that subboundaries have migrated.

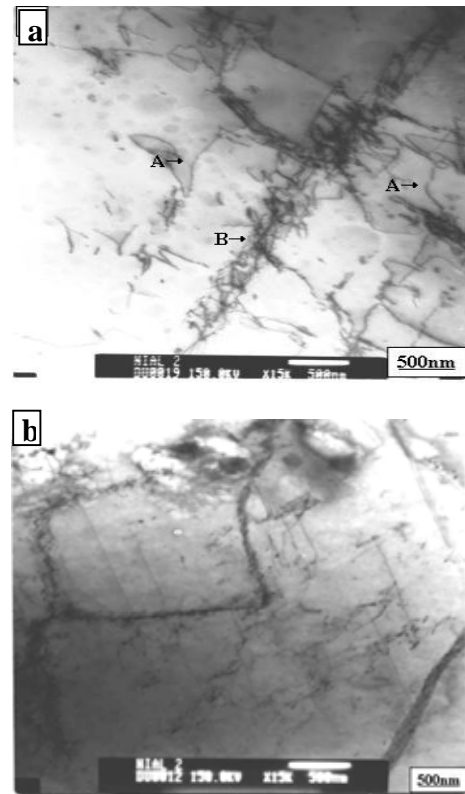


Fig. 7. Dislocation network and subboundary configuration in the sample deformed at 1373 K up to an elongation of 40%

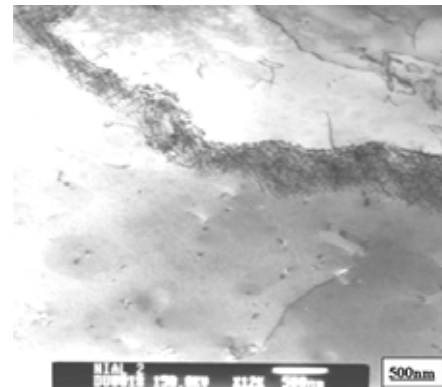


Fig. 8. Configuration of the migrated subboundaries in the sample deformed at 1373 K up to an elongation of 210%

To study the dislocation configuration of the subboundary, contrast analysis has been performed in the present study. As shown in Fig. 9, the dislocations were labeled as 1,2. When the operation  $g=0\bar{1}1$ , all dislocations were in contrast (Fig.9 (a)), but when  $g=002$ , all the dislocations were out of contrast (Fig.9 (d)). When  $g=020$ , the dislocations labeled as 1 were in contrast but the others were out of contrast (Fig.9

(b)). When  $g=1\bar{1}0$ , the dislocations labeled as 2 were in contrast but the others were out of contrast (Fig.9 (c)). Forgoing contrast analyses obviously showed that the Burgers vector of the dislocations labeled as 1 was  $a[100]$ , and that of the other was  $a[110]$ . Therefore, the boundary of recrystallized grain was composed of  $a[100]$  and  $a[110]$  dislocations. Similar analyses were also appeared to the tangled dislocations as well as to discrete dislocations. While most of these dislocations were found to have the Burgers vector  $a[100]$ , very few dislocation were found have an Burgers vectors  $a[110]$ . So the dislocations labeled as 2 in the boundary were junction dislocations, resulting from elastically favorable interactions of type:

$$a[100]+a[010]=a[110] \quad (3)$$

The  $[100]$  edge dislocation first arranged as a dislocation arrayed to construct a skeleton of subboundary and other glided  $[010]$  dislocation could be attracted by the boundary to combine with the  $[100]$  dislocation to create new  $[110]$  dislocation. The absorption of dislocations in subboundaries may result in the increase of the dislocation density on the boundary. As a result, the misorientation between two subgrains increased with the ongoing of the deformation process. Here, two points should be stressed: first point was that the dislocation density within the subgrain as well as in the whole microstructure was still very high (Fig.7 (d)). The second point was that the subgrain boundaries were developed along the normal direction to  $\langle 100 \rangle$  but formed by the combination of a number of edge dislocations of the  $\langle 100 \rangle$  and  $\langle 110 \rangle$  dislocations. However, very few slid  $\langle 110 \rangle$  dislocations were discovered.

Based on the forgoing observations, the evolution of the dislocation structure in NiAl during the superplastic deformation process could be described as follows.

1. At the initial stage of deformation, corresponding to the rapid strain hardening, the glide of  $\langle 100 \rangle$  type dislocations was dominant in the microstructure of NiAl.
2. With the increase of strain, the dislocation density increased. At this stage, the gliding dislocations arranged themselves as arrays to form subboundaries and the initially large grains were gradually divided into numerous small subgrains.
3. With further deformation, the newly created  $\langle 100 \rangle$  type dislocations in the subgrains were absorbed by the subboundaries by climb, dislocations reactions based on Eqs. (3) occurred and resulted in the formation of dislocations of  $\langle 110 \rangle$  type. They arranged themselves as one part of subboundaries, and misorientation increased.

4. The subboundaries evolved into low angle grain boundaries and even to high angle boundaries with increase of strain. This means continuous dynamic recrystallization (CDRX) occurred. In the course of deformation, the evolution of subboundaries to grain boundary should contribute to superplastic deformation.

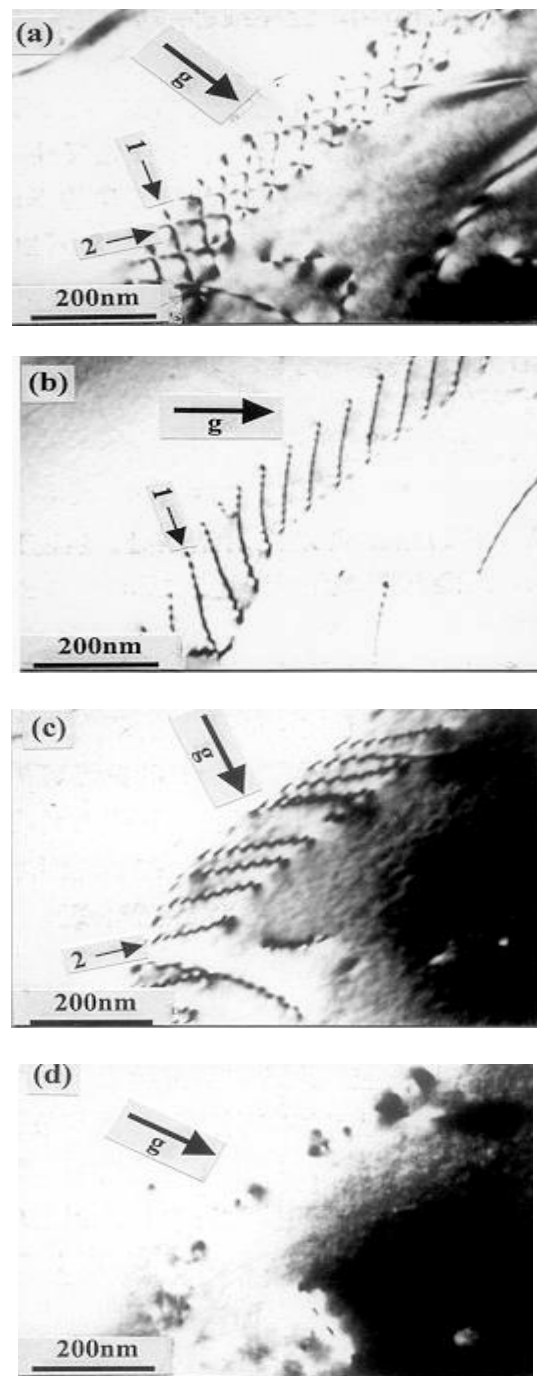


Fig.9. The subgrain boundary composed of  $[001]$  and  $[110]$  dislocations, weak-beam  $1g/3g$  conditions.

## DEFORMATION PROCESS

It is well known that the method of TEM is difficult to characterize the whole microstructures during deformation because of its limited observation area. The most recently developed scanning electron microscope (SEM)-based electron back-scattered diffraction (EBSD) technique may solve this problem very well [16-17]. The technique is effective and useful not only in determining the orientation and phase of individual grains and the distribution of grain misorientations but also in identifying the type of grain boundaries. So in this paper, EBSD technique is used to describe CDRX occurred in superplastic deformation on NiAl by clarifying the evolution process of recrystallized grain.

### 3.3.3 EBSD observations

Fig. 10 showed EBSD orientation-mapping images taken from the gauge section of the specimens deformed with a strain rate of  $1.67 \times 10^{-2} \text{ s}^{-1}$  at 1273 K with different strain values. In the mapping images, black lines represent the subgrain and grain boundaries having misorientation angles of  $2 \sim 10^\circ$  (low angle boundaries), whereas red lines are used for misorientation angles of more than  $15^\circ$  (high angle boundaries). The bright green lines represent the grain boundaries having misorientation angles of  $10 \sim 15^\circ$ . Fig. 10 showed the EBSD observations corresponding to the sample deformed up to 40% (a) and 200% (b). In Fig. 10 (a), the initial large grains bordered by high angle grain boundaries have been found. From Fig. 10 (b), it can be seen that the grain sizes in the samples were dramatically refined after deformation because red line bordered small-area scope. Furthermore, the density of low angle grain boundaries with the misorientation between  $2$  to  $10^\circ$  in the sample after deformation to 200% was much higher than those in the sample after deformation to 40%. The density of low angle grain boundary was much higher in the sample after deformation than that in the sample before deformation, indicating that CDRX was connected with the whole deformation process. It is important to observe the emergence of intermediate boundary with the angle of  $10 \sim 15^\circ$  in the grain (bright green line), which proved that the high angle boundaries evolved from low angle boundaries. Fig. 11(a) and (b) show that the standard orientation triangles corresponding to Fig. 10 (a) and (b), respectively, in which the orientation represented by each kind of color can be identified.

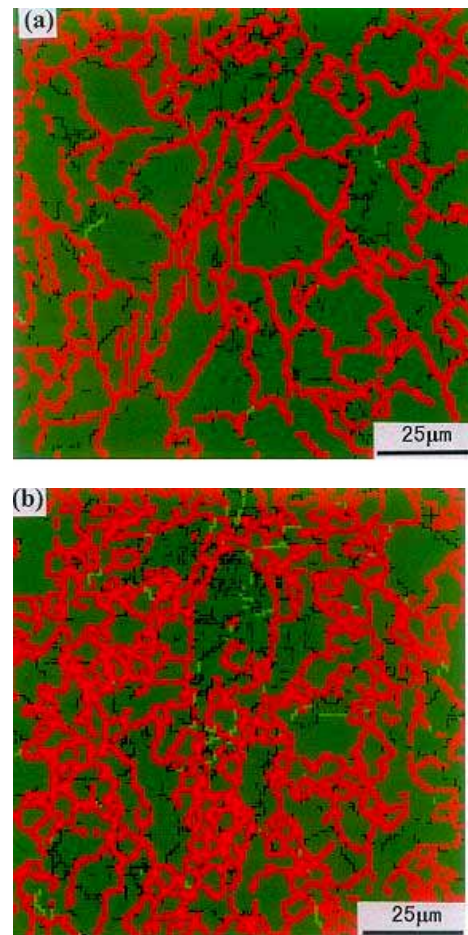


Fig.10. EBSD orientation-mapping images of gauge regions of specimens deformed at 1273 K and a strain rate of  $1.67 \times 10^{-2} \text{ s}^{-1}$  with up to elongations of 40% (a) and 200% (b).

## 4. Discussion

### 4.1 Analysis of deformation behavior

Careful inspection of the deformation behavior of extruded NiAl polycrystalline specimens has shown that the value of the apparent activation energy for superplastic deformation was in good agreement with the value of the activation energy for vacancy migration in NiAl. The value of  $Q = 260 \text{ kJ/mol}$  can be interpreted in terms of high temperature dislocation climb, as a controlling process for superplastic deformation. However, the stress exponent,  $n \sim 3$  is not consistent with high temperature climb. It is seen that deformation behavior of extruded polycrystalline NiAl is very complicated and there is not an ambiguity in its interpretation. It is possible to presume that the deformations at 1273 or 1373 K at strain rates of  $10^{-5} \sim 10^{-1} \text{ s}^{-1}$  fall into the range of high-temperature deformation, where intense dislocation climb takes

place, as TEM observations have shown. This type of dislocation climb is controlled by vacancy diffusion along dislocation cores and may cause dislocation rearrangement at small distances. In addition, it can be concluded from TEM observations that glide of dislocation also plays an important role in dislocation rearrangements. The results obtained indicate that the dynamic recovery occurring at high temperatures is not so extensive to reduce significantly the dislocation density stored during deformation. Therefore, the steady state flow stress could be associated with the occurrence of a recrystallization process originated from dynamic recovery, i.e. continuous dynamic recrystallization (CDRX).

#### 4.2 CDRX

Based on the forgoing observations and analysis, during superplastic deformation of NiAl, the localization of dislocation glide resulted in the formation of subboundaries and then highly stable low angle boundaries. In the regions of localized deformation, the forming of pile-ups of lattice dislocations belonging to  $\{100\}$  [100] and  $\{100\}$ [110] systems could play a role of barriers for mobile dislocations of  $\{100\}$ [100]. As a result, an extensive accumulation of dislocations with [100] Burgers vectors took place here [Fig.12]. Following dislocations, rearranged by glide and climb yielded the formation of longitudinal subboundaries. Such longitudinal subboundaries were characterized by low mobility and had non-compensated long-range stress field [18]. The formation of such subboundaries would initiate CDRX. Long-range non-compensated stress fields originating from the longitudinal subboundaries interact with short-range stress field originating from other deformation induced low angle boundaries. Following deformation resulted in the formation of transverse subboundaries in the areas of localized deformation. Mobile lattice dislocations introduced into low angle boundaries during subsequent deformation, which caused an increase of dislocation density of subboundaries, and low angle boundaries eventually converted to high angle boundaries. Subsequent grain boundary migration provided the formation of an equilibrium network of high-angle boundaries, as shown in Fig.8 (b). As a result, the subgrains gradually evolved into equiaxed recrystallized grains with strain. The new grains formed have the equilibrium shape and coarsen significantly during the last stage.

The results presented prove that continuous dynamic recrystallization (CDRX) has occurred in the B2 typed NiAl polycrystalline during superplastic deformation at elevated temperatures. CDRX was observed in numerous metals with high stacking fault energies at

high temperature [19-22], and the evolution of CDRX can be summarized as follows process:

- (1) stable subgrain structure forms at low strains;
  - (2) part of low-angle boundaries gradually evolve into high-angle grain boundaries by dislocation accumulation during superplastic deformation;
- migration of new grain boundaries occurs at the same time.

Fig.11 can be used to describe the microstructural evolution in extruded NiAl deformed at 1100 . The formation of a well-defined subgrain structure and subsequent conversion of low angle into high angle boundaries take place at the steady state of plastic deformation. Onset of CDRX results in the establishment of steady state of plastic deformation at which a dynamic equilibrium between hardening by dislocation glide and softening by dynamic recrystallization exists. Therefore, CDRX can weaken internal stress then promote further dislocation motion besides accommodating grain compatibility in NiAl. On the other hand, CDRX is a dynamic event during deformation, making the necking unlikely to form. Accordingly, the synchronous operation of dislocation glide and CDRX were responsible for extruded NiAl polycrystalline to be superplastic.

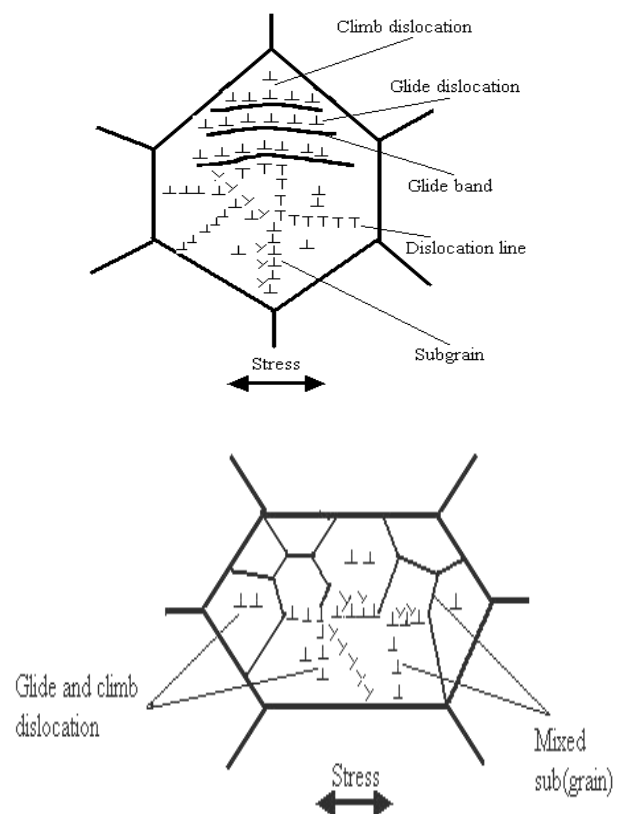


Fig. 11 Schematic representation of structural evolution in extruded NiAl during deformation (a) the formation of subgrain structure at the initial deformation stage, (b) the formation of mixed (sub)grain structure.

## 5. Summary and Conclusions

The microstructural evolution and mechanical properties of conventional cast and hot extruded NiAl with stoichiometric composition have been characterized. The obtained material exhibited superplastic deformation at a relatively wide strain rate range ( $10^{-4}\text{ s}^{-1}\sim 10^{-1}\text{ s}^{-1}$ ) above 1273 K. It is promising to discover the superplastic deformation for NiAl at very high strain rate of  $10^{-1}\text{ s}^{-1}$ , which can be used in conventional industry directly. Based on OM, TEM and EBSD observations, continuous dynamic recrystallization was found to occur in polycrystalline NiAl during the superplastic deformation process. The results can be summarized as follow:

- 1) Subgrain formed by dynamic recovery during an initial stage of superplastic deformation. Subgrain boundaries acted as sinks for gliding dislocations generated during the whole deformation process via climb mechanism, resulting in an increase in misorientation of subgrains.
- 2) With further deformation, more low or high angled grains formed, therefore the microstructure was dramatically refined. On the other hand, the recrystallized grains coarsened continuously, although they were much fine in size than those of parent grains.
- 3) Continuous dynamic recrystallization was a dynamic event during deformation, making the necking unlikely to form. Both dislocation behavior and continuous dynamic recrystallization were responsible for extruded polycrystalline NiAl to be superplastic.

## Acknowledgements

Dr. V. Lupinc and E. Signorelli of Istituto Per I ' Energetica ele Interfasi of Italy are sincerely thanked for their assistance in OM and TEM observations by the authors. The support of this research by the Natural Science Foundation of China (contract No.59895152 and 59801010) and the National Advanced Materials Committee of China (No. 863-715-0030) is gratefully acknowledged.

## References

- [1] D.R. Miracle. The Physical and Mechanical Properties of NiAl. *Acta Metall. Mater*, Vol. 41, No.3, pp 649-684, 1993.
- [2] R.D. Noebe, R.R. Bowman, M.V. Nathal. Physical and Mechanical Properties of the B2 Compound NiAl. *International Materials Reviews*, Vol.38, No.4, pp 193-232, 1993.
- [3] A.G. Rozner, R.J. Wasilewski. Tensile Properties of NiAl and NiTi. *Journal of the Institute of Metals*, Vol.34, pp 169-175, 1966.
- [4] R.D.Noebe, C.L. Cullers, R.R. Bowman. The Effect of Strain Rate and Temperature on the Tensile Properties of NiAl. *Journal of Materials Research*, Vol.7, No.3, pp 605-611, 1992.
- [5] T.Takasugi, J.Kishino, S. Hanada. Anomalous Elongation Behavior of Stoichiometric NiAl Single Crystals at Intermediate Temperature. *Acta Metallurgica et Materialia*, Vol.41, No.4, pp 1009-1020, 1993.
- [6] M.H.Loretto, R.J.Wasilewski. Slip System in NiAl Single Crystals at 300 K and 77 K. *The Philosophical Magazine*, Vol.23, No.186, pp 1311-1328, 1971.
- [7] R.J. Wasilewski, S.R. Butler, J.E. Hanlon. Plastic deformation of Single-crystal NiAl. *Transactions of the Metallurgical Society of AIME*, Vol. 239, pp 1357-1364, 1967.
- [8] R.R. Bowman, R.D. Noebe, S. V. Rai, I.E. Locci. Correlation of Deformation Mechanisms with the Tensile and Compressive Behavior of NiAl and NiAl(Zr) Intermetallic Alloys. *Metallurgical Transaction A*, Vol.23A, No.5, pp 1493-1507, 1992.
- [9] R.D. Noebe, R.Gibala. Surface Oxide Softening of Single Crystal NiAl. *Scripta Metallurgica*, Vol.20, No.11, pp 1635-1639, 1986.
- [10] A. Ball, R.E. Smallman. The Deformation Properties and Electron Microscopy Studies of the Intermetallic Compound NiAl. *Acta Metallurgica*, Vol.14, No.7, pp 1349-1361, 1966.
- [11] X.H.Du, J.T.Guo, B.D.zhou. Superplasticity of Stoichiometric NiAl with large Grains. *Scripta Materialia*, Vol.45, No.1, pp 69-74, 2001.
- [12] R.T. Pascoe, C.W.A. Newey. Deformation Nodes of the Intermediate Phase NiAl. *Physica Status Solidi (a)*, Vol.29, No.1, pp 357-366, 1968.
- [13] Mills M J, Miracle D B. The Structure of a <100> and a <110> Dislocation Cores in NiAl. *Acta Metallurgica et Materialia*, Vol.41, No.1, pp 85-96, 1993.
- [14] Oleg D. Sherby, Jeffrey Wadsworth. Superplasticity-Recent Advances and Future Directions. *Progress in Materials Science*, Vol.33, No.3, pp 169-221, 1989.
- [15] T. G. Nieh, J. Wadsworth. Fine structure superplastic Intermetallics. *International Materials Reviews*, Vol.44, No.2, pp 59-75, 1999.
- [16] M.R. Barnett, F. Montheillet. The generation of new high-angle boundaries in aluminium during hot torsion. *Acta Materialia*, Vo.50, No. 9, pp 2285-2296, 2002.
- [17] J.P. Chu, J.H. Wu, H.Y. Yasuda, Y. Umakoshi, K. Inoue. Electron backscattered diffraction study on superplastic properties of coarse-grained Fe-27 at% Al. *Intermetallics*, Vol.8, No.1, pp 39-46, 2000.
- [18] H. Mughrabi. Dislocation Wall and Cell Structures

- and Long-range Internal Stress in Deformed Metal Crystals. *Acta Metallurgica*, Vol.31, No.9, pp 1376-1386, 1983.
- [19] S.J. Hales, T.R. McNelly. Microstructural Evolution by Continuous Recrystallization in A superplastic Al-Mg alloy. *Acta Metallurgica*, Vol.36, No.5, pp 1229-1239, 1988.
- [20] A. Belyakov, R. Kaibyshev. The Characterization of Microstructural Evolution of Zn Alloys During High-temperature Deformation. *Phys.Met.Metallogr*, Vol.78, No.1, pp 91-99, 1994.
- [21] J.C. Tan, M.J. Tan. Dynamic continuous recrystallization characteristics in two stage deformation of Mg-3Al-1Zn alloy sheet. *Materials Sciences and Engineering*, Vol. 339 A, No.1-2, pp 124-132, 2003.
- [22] Gourdet S, Montheillet F. An experimental study of the recrystallization mechanism during hot deformation of aluminium. *Materials Sciences and Engineering*, Vol.283 A, No.1-2, pp 274-288, 2000.